Surface Fermi arcs in $\mathbb{Z}_2$ Weyl semimetals A_3Bi (A = Na, K, Rb)

E. V. Gorbar,[1,2] V. A. Miransky,[3,4] I. A. Shovkovy,[5] and P. O. Sukhachov[1]
[1]*Department of Physics, Taras Shevchenko National Kiev University, Kiev 03680, Ukraine*
[2]*Bogolyubov Institute for Theoretical Physics, Kiev 03680, Ukraine*
[3]*Department of Applied Mathematics, Western University, London, Ontario, Canada N6A 5B7*
[4]*Department of Physics and Astronomy, Western University, London, Ontario, Canada N6A 3K7*
[5]*College of Letters and Sciences, Arizona State University, Mesa, Arizona 85212, USA*
(Received 31 March 2015; revised manuscript received 5 June 2015; published 22 June 2015)

The surface Fermi arc states in $\mathbb{Z}_2$ Weyl semimetals A_3Bi (A = Na,K,Rb) are studied by employing a continuum low-energy effective model. It is shown that the surface Fermi arc states can be classified with respect to the ud-parity symmetry. Because of the symmetry, the arcs come in mirror symmetric pairs. The effects of symmetry breaking terms on the structure of the Fermi arcs are also studied. Among other results, we find at least two qualitatively different types of the surface Fermi arcs. The arcs of the first type link *disconnected* sheets of the bulk Fermi surface, while arcs of the second type link different points of the *same* bulk Fermi surface sheet.

DOI: 10.1103/PhysRevB.91.235138 PACS number(s): 73.20.At, 71.10.−w, 03.65.Vf

I. INTRODUCTION

3D Dirac semimetals are 3D analogs of graphene [1]. Their conduction and valence bands touch only at discrete (Dirac) points in the Brillouin zone with the electron states described by the 3D massless Dirac equation. Each Dirac point in momentum space is composed of two superimposed Weyl nodes of opposite chirality. Such points are usually obtained by fine tuning of certain physical parameters (e.g., the spin-orbit coupling strength or chemical composition) and are difficult to control. Additionally, they are often unstable with respect to mixing of Weyl modes and opening a gap.

An important idea was proposed in Refs. [2,3], where it was shown that an appropriate crystal symmetry can protect and stabilize the gapless 3D Dirac points. Indeed, if a pair of crossing bands belong to different irreducible representations of the discrete (rotational) crystal symmetry and if this symmetry is not broken dynamically, then the mass term for the corresponding Dirac fermions will be prohibited. The *ab initio* calculations in Ref. [2] showed that β-cristobalite BiO_2 exhibits three Dirac points at the Fermi level. Unfortunately, this material is metastable. By using first-principles calculations and an effective model analysis, the compounds A_3Bi (A = Na, K, Rb) and Cd_3As_2 were identified in Refs. [4,5] as possible 3D Dirac semimetals protected by crystal symmetry. Giant diamagnetism, linear quantum magnetoresistance, and the quantum spin Hall effect are expected in these materials. Furthermore, various topologically distinct phases can be realized in these compounds by breaking the time-reversal and inversion symmetries. By using angle-resolved photoemission spectroscopy, the Dirac semimetal band structure was indeed observed [6–8] in Cd_3As_2 and Na_3Bi opening the path toward experimental investigations of the properties of 3D Dirac semimetals.

Weyl semimetals is another group of materials that is closely related to 3D Dirac semimetals and have already attracted a lot of theoretical interest (for reviews, see Refs. [9–11]). They are characterized by topologically nontrivial Weyl nodes in reciprocal space. Weyl nodes are monopoles of the Berry flux and, therefore, can appear or annihilate only in pairs. Weyl semimetals were proposed to be realized in pyrochlore iridates [12], topological heterostructures [13], magnetically doped topological insulators [14], and nonmagnetic materials such as TaAs [15,16]. Recently, first experimental studies of Weyl semimetal candidate TaAs were reported in Refs. [17–20]. The authors observed unusual transport properties and surface states that are characteristic of the Weyl semimetal phase. Another interesting realization of the Weyl points in the context of photonic crystals has been recently reported in Ref. [21].

Since the magnetic field breaks the time-reversal symmetry, a Dirac (semi-)metal in a magnetic field may transform into a Weyl one with Weyl nodes separated in momentum space by a nonzero chiral shift [22]. Experimentally, the transition from a Dirac metal to a Weyl one in a magnetic field might have been observed in $Bi_{1-x}Sb_x$ for $x \approx 0.03$ [23]. In moderately strong magnetic fields, a negative magnetoresistivity is observed and interpreted as a fingerprint [24–26] of a Weyl/Dirac metal phase.

The surface Fermi arcs [12,27–29], which connect Weyl nodes of opposite chirality, are related to the nontrivial topology of Weyl semimetals. In equilibrium, the presence of such surface states ensures that the chemical potentials at different Weyl points are identical [27]. Although Fermi arcs always connect Weyl nodes of opposite chirality, their shapes depend on the boundary conditions and, as shown in Ref. [30], Fermi arcs of an arbitrary form can be engineered. The Fermi arcs on the opposite surfaces of a semimetal sample together with the Fermi surfaces of bulk states form a closed Fermi surface. In an external magnetic field, the nontrivial structure of the corresponding Fermi surface gives rise to closed magnetic orbits involving the surface Fermi arcs [31]. These orbits produce periodic quantum oscillations of the density of states in a magnetic field leading to unconventional Fermiology of surface states. It was argued in Ref. [32] that the interaction effects can change the separation between Weyl nodes in momentum space and the length of the Fermi arcs in the reciprocal space and, thus, affect these magnetic orbits. As a result, we found that the period of oscillations of the density of states related to closed magnetic orbits involving Fermi arcs has a nontrivial dependence on the orientation of the magnetic field projection in the plane of the semimetal surface [32]. If experimentally observed, such a dependence would provide an important clue to the effects of interactions in Weyl semimetals.

Normally, one would not expect any surface Fermi arcs in 3D Dirac semimetals because the Dirac point has no topological charge and the associated Berry flux vanishes. In Refs. [4,5], however, it was shown that the 3D Dirac semimetals A_3Bi (A = Na,K,Rb) and Cd_3As_2 possess nontrivial surface Fermi arcs. This finding suggests a topologically nontrivial nature of the corresponding Dirac materials. Recently, we showed [33] that this is indeed the case for Dirac semimetals A_3Bi (A = Na,K,Rb). The physical reason for their nontrivial topological properties is connected with a discrete symmetry of the low-energy effective Hamiltonian. The symmetry classification allows one to split all electron states into two separate sectors, each describing a Weyl semimetal with a pair of Weyl nodes and broken time-reversal symmetry. The time-reversal symmetry is preserved in the complete theory because its transformation interchanges states from the two different sectors. The nontrivial topological structure of each sector was supported by explicit calculations of the Berry curvature, which revealed a pair of monopoles of the Berry flux at the positions of Weyl nodes in each of the two sectors of these semimetals [33]. In essence, these results demonstrated that Dirac semimetals A_3Bi (A = Na,K,Rb) are, in fact, $\mathbb{Z}_2$ Weyl semimetals.

In Refs. [4,5], the surface Fermi arcs in 3D Dirac semimetals were obtained in a tight-binding model by using an iterative method that produces the surface Green's function of the semi-infinite system [34]. The imaginary part of the surface Green's function makes possible to determine the local density of states at the surface. While such a technique is very powerful, it is essentially a "black box." In contrast, in the present paper, we study analytically the surface Fermi arc states by employing the continuum low-energy effective model with appropriate boundary conditions at the surface. We hope that such a consideration will provide a deeper understanding of the physical properties and characteristics of the surface Fermi arcs, as well as shed more light on the nontrivial topological properties of the A_3Bi compounds.

The paper is organized as follows. In Sec. II, we introduce the low-energy effective model and discuss its symmetries. The recently revealed $\mathbb{Z}_2$ Weyl semimetal structure of A_3Bi (A = Na, K, Rb) is emphasized. In order to clarify the origin and the structure of the surface Fermi arcs, we study in Sec. III the corresponding states in a simplified model that contains a single Weyl semimetal sector. In Sec. IV, we present the rigorous analysis of the surface Fermi arc states in a realistic low-energy model of semimetals A_3Bi (A = Na,K,Rb). The effects of several possible symmetry breaking terms on the structure of the surface Fermi arc states are investigated in Sec. V. The discussion and the summary of the main results are given in Sec. VI. Technical details regarding the symmetry properties and classification of the Fermi arc states are presented in Appendixes A and B.

For convenience, throughout the paper, we set $\hbar = 1$ and $c = 1$.

II. MODEL

A. Low-energy effective Hamiltonian

The low-energy Hamiltonian derived in Ref. [4] for A_3Bi (A = Na,K,Rb) has the form

$$H(\mathbf{k}) = \epsilon_0(\mathbf{k}) + H_{4\times4}, \tag{1}$$

where $\epsilon_0(\mathbf{k}) = C_0 + C_1k_z^2 + C_2(k_x^2 + k_y^2)$ and

$$H_{4\times4} = \begin{pmatrix} M(\mathbf{k}) & Ak_+ & 0 & B^*(\mathbf{k}) \\ Ak_- & -M(\mathbf{k}) & B^*(\mathbf{k}) & 0 \\ 0 & B(\mathbf{k}) & M(\mathbf{k}) & -Ak_- \\ B(\mathbf{k}) & 0 & -Ak_+ & -M(\mathbf{k}) \end{pmatrix}. \tag{2}$$

While the diagonal elements of $H_{4\times4}$ are given in terms of a single function, $M(\mathbf{k}) = M_0 - M_1k_z^2 - M_2(k_x^2 + k_y^2)$, the off-diagonal elements are determined by functions $Ak_\pm$ and $B(\mathbf{k}) = \alpha k_z k_+^2$, where $k_\pm = k_x \pm ik_y$.

By fitting the energy spectrum of the effective Hamiltonian with the *ab initio* calculations, the numerical values of parameters in the effective model were determined in Ref. [4]. They are

$$\begin{aligned} &C_0 = -0.06382 \text{ eV}, \quad C_1 = 8.7536 \text{ eV Å}^2, \quad C_2 = -8.4008 \text{ eV Å}^2, \\ &M_0 = -0.08686 \text{ eV}, \quad M_1 = -10.6424 \text{ eV Å}^2, \quad M_2 = -10.3610 \text{ eV Å}^2, \\ &A = 2.4598 \text{ eV Å}, \quad a = 5.448 \text{ Å}, \quad c = 9.655 \text{ Å}, \end{aligned} \tag{3}$$

where we also included the lattice constants a and c. Since no specific value for α was quoted in Ref. [4], we will treat it as a free parameter below.

The energy eigenvalues of the low-energy Hamiltonian (1) are given by the following explicit expression:

$$E(\mathbf{k}) = \epsilon_0(\mathbf{k}) \pm \sqrt{M^2(\mathbf{k}) + A^2k_+k_- + |B(\mathbf{k})|^2}. \tag{4}$$

It is easy to check that the term with the square root vanishes at the two Dirac points, $\mathbf{k}_0^\pm = (0,0,\pm\sqrt{m})$, where $\sqrt{m} \equiv \sqrt{M_0/M_1}$. With the choice of the low-energy parameters in Eq. (3), we find that $\sqrt{m} \approx 0.09034$ Å^{-1}. The function $B(\mathbf{k})$ plays the role of a momentum dependent mass (gap) function that vanishes at the Dirac points.

It is instructive to show that linearizing $M(\mathbf{k})$ in the vicinity of the Dirac points $\mathbf{k}_0^\pm$, Hamiltonian (2) takes the form of a 3D massive Dirac Hamiltonian. In the vicinity of $\mathbf{k}_0^-$, expanding $M(\mathbf{k})$ to the linear order in $\delta\mathbf{k} = \mathbf{k} - \mathbf{k}_0^-$, we obtain

$$H_{4\times4}^{\text{lin}} = \begin{pmatrix} A(\tilde{k}_x\sigma_x - \tilde{k}_y\sigma_y - \tilde{k}_z\sigma_z) & B^*(\mathbf{k})\sigma_x \\ B(\mathbf{k})\sigma_x & -A\,\tilde{\mathbf{k}}\cdot\boldsymbol{\sigma} \end{pmatrix}, \tag{5}$$

where $\boldsymbol{\sigma}$ are Pauli matrices and $\tilde{\mathbf{k}} = (k_x, k_y, 2\delta k_z\sqrt{M_0M_1}/A)$. Furthermore, by performing the unitary transformation, $\tilde{H}_{4\times4}^{\text{lin}} \equiv U_x^+ H_{4\times4}^{\text{lin}} U_x$, where $U_x = \text{diag}(\sigma_x, I_2)$ and I_2 is the 2×2 unit matrix, we find that the Hamiltonian takes the

standard form of the Dirac Hamiltonian in the chiral representation,

$$\tilde{H}^{\rm lin}_{4\times4} = \begin{pmatrix} A\,\tilde{\mathbf{k}}\cdot\boldsymbol{\sigma} & B^*(\mathbf{k}) \\ B(\mathbf{k}) & -A\,\tilde{\mathbf{k}}\cdot\boldsymbol{\sigma} \end{pmatrix}. \tag{6}$$

Taking into account that the mass term $B(\mathbf{k})$ vanishes at the Dirac point, we conclude that the upper and lower 2×2 blocks describe quasiparticle states of opposite chiralities. Also, since the leading order nonzero corrections to the mass function are quadratic in momentum, the chirality remains a good quantum number in a sufficiently small vicinity of the Dirac point. Hamiltonian (6), describing two subsets of the opposite chirality states near a single Dirac point, does not appear to have any interesting topological properties. Also, by itself, it is unlikely to give rise to any Fermi arcs states. It is easy to check, however, that Hamiltonian (2) linearized near $\mathbf{k}_0^+$ has a similar structure and describes two additional subsets of the opposite chirality states. As we argue below, the superposition of the two sectors of the theory is nontrivial and gives rise to an interesting topological structure [33].

B. Symmetries

Let us briefly review the symmetry properties of the low-energy Hamiltonian following Ref. [33]. We start by pointing out that, as expected, the Hamiltonian (1) is invariant under the time-reversal and inversion symmetries, i.e.,

$$\Theta H_{-\mathbf{k}}\Theta^{-1} = H_{\mathbf{k}} \quad \text{(time-reversal symmetry)}, \tag{7}$$

$$P H_{-\mathbf{k}} P^{-1} = H_{\mathbf{k}} \quad \text{(inversion symmetry)}, \tag{8}$$

where $\Theta = TK$ (K is complex conjugation) and

$$T = \begin{pmatrix} 0 & 0 & 1 & 0 \\ 0 & 0 & 0 & 1 \\ -1 & 0 & 0 & 0 \\ 0 & -1 & 0 & 0 \end{pmatrix}, \quad P = \begin{pmatrix} 1 & 0 & 0 & 0 \\ 0 & -1 & 0 & 0 \\ 0 & 0 & 1 & 0 \\ 0 & 0 & 0 & -1 \end{pmatrix}. \tag{9}$$

Having both, the time-reversal and inversion symmetries, suggests that the corresponding compounds are not Weyl semimetals. This is not the whole story, however.

As shown in Ref. [33], the low-energy Hamiltonian in Eq. (1) possesses a new discrete symmetry, the so-called up-down parity (ud-parity), that protects its topological nature. In order to understand the corresponding symmetry, it is instructive to start from the approximate Hamiltonian without the mass function $B(\mathbf{k})$ (or, alternatively, $\alpha = 0$). In this case, the 4×4 Hamiltonian takes a block diagonal form: $H_{4\times4}(\alpha=0) \equiv H^+_{2\times2} \oplus H^-_{2\times2}$. The explicit form of the upper block is given by

$$H^+_{2\times2} = \begin{pmatrix} M_0 - M_1k_z^2 - M_2\left(k_x^2+k_y^2\right) & A(k_x+ik_y) \\ A(k_x-ik_y) & -\left[M_0 - M_1k_z^2 - M_2\left(k_x^2+k_y^2\right)\right] \end{pmatrix}. \tag{10}$$

This block Hamiltonian defines a Weyl semimetal with two Weyl nodes located at $\mathbf{k}_0^\pm$. (The lower block $H^-_{2\times2}$ has a similar form, except that k_x is replaced by $-k_x$.) It is well known [29,31] that such a Weyl semimetal has the surface Fermi arc connecting the Weyl nodes of opposite chirality at $\mathbf{k}_0^+$ and $\mathbf{k}_0^-$. Because of the sign difference, $k_x \to -k_x$, the chiralities of the states near the Weyl nodes at $\mathbf{k}_0^\pm$ are opposite for the upper and lower block Hamiltonians. Thus the complete 4×4 block diagonal Hamiltonian $H_{4\times4}(\alpha=0)$ describes two superimposed copies of Weyl semimetal with two pairs of overlapping nodes. Since the opposite chirality Weyl nodes coincide exactly in momentum space, they effectively give rise to a pair of Dirac points at $\mathbf{k}_0^\pm$. At the same time, because the opposite chirality nodes come from two different Weyl copies, they cannot annihilate and cannot form topologically trivial Dirac points. In fact, the corresponding approximate model describes a $\mathbb{Z}_2$ Weyl semimetal [33]. The nontrivial topological properties, associated with the underlying $\mathbb{Z}_2$ Weyl semimetal structure, ensure that the resulting Dirac semimetal possesses surface Fermi arcs.

It is easy to show that the existence of the $\mathbb{Z}_2$ Weyl semimetal structure in the absence of $B(\mathbf{k})$ is connected with the continuous symmetry $\mathrm{U}_+(1)\times\mathrm{U}_-(1)$ of the approximate Hamiltonian $H_{4\times4}(\alpha=0)$. This symmetry describes independent phase transformations of the spinors that correspond to the up- and down-block Hamiltonians, $H^+_{2\times2}$ and $H^-_{2\times2}$, respectively.

For $B(\mathbf{k}) \neq 0$, the continuous symmetry $\mathrm{U}_+(1)\times\mathrm{U}_-(1)$ is broken down to its diagonal subgroup $\mathrm{U}_{\rm em}(1)$ that describes the usual charge conservation. However, the low-energy Hamiltonian (1) with the momentum dependent mass function $B(\mathbf{k}) = \alpha k_z k_+^2$ possesses a ud-parity, defined by the following transformation [33]:

$$U H_{-k_z} U^{-1} = H_{k_z} \quad \text{(ud-parity)}, \tag{11}$$

where matrix U has the following block diagonal form: $U \equiv \mathrm{diag}(I_2, -I_2)$ and I_2 is the 2×2 unit matrix. For the Hamiltonian to be symmetric under the ud-parity, it is crucial that the mass function $B(\mathbf{k})$ changes its sign when $k_z \to -k_z$ [while the functions $\epsilon_0(\mathbf{k})$ and $M(\mathbf{k})$ in the diagonal elements do not change their signs]. In the special case of a momentum independent mass function, such a discrete symmetry does not exist.

As was argued in Ref. [33], the existence of the noncommuting time-reversal and ud-parity symmetries implies that the A_3Bi semimetal is, in fact, a $\mathbb{Z}_2$ Weyl semimetal. In such a semimetal, all quasiparticle states can be split into two separate groups, labeled by the eigenvalues $\chi = \pm1$ of $U_\chi = U\Pi_{k_z}$, where Π_{k_z} is the operator that changes the sign of the z component of momentum, $k_z \to -k_z$. Effectively, each group of states defines a Weyl semimetal with a broken time-reversal symmetry. The corresponding symmetry is preserved in the complete theory, in which the two copies of Weyl semimetals are superimposed.

The $\mathbb{Z}_2$ Weyl semimetal structure of A_3Bi ($A = Na, K, Rb$) is also supported by the explicit calculation of the Berry connection and the Berry curvature in each Weyl sector described [33]. In particular, the corresponding results for the curvature in the momentum space reveal a clear dipole structure. It is natural, that each Weyl sector, described by quasiparticle states with a fixed eigenvalue of U_χ, should give rise to Fermi arcs connecting the pairs of Weyl nodes at $\mathbf{k}_0^{\pm}$. Moreover, such arcs should be topologically protected and could not be removed by small perturbations of model parameters.

In our discussion of Fermi arcs below, it will be also useful to take into account that there exists yet another discrete symmetry defined by the following transformation:

$$\tilde{U} H_{-k_x} \tilde{U}^{-1} = H_{k_x}, \tag{12}$$

where

$$\tilde{U} = \begin{pmatrix} 0 & 0 & 1 & 0 \\ 0 & 0 & 0 & 1 \\ 1 & 0 & 0 & 0 \\ 0 & 1 & 0 & 0 \end{pmatrix}. \tag{13}$$

It is interesting to note that the product of the U_χ and $\tilde{U}\Pi_{k_x}$ transformations $U_\chi \tilde{U}\Pi_{k_x} = T\Pi_{k_x}\Pi_{k_z}$ is also a symmetry of the low-energy Hamiltonian (1). The symmetry $T\Pi_{k_x}\Pi_{k_z}$ is related to the time-reversal symmetry. This follows from the fact that $K\Pi_{k_y}$ is also the symmetry of the low-energy Hamiltonian (1). Together the operators U_χ, $\tilde{U}\Pi_{k_x}$, and $T\Pi_{k_x}\Pi_{k_z}$ form a noncommutative discrete group.

Hamiltonian (1) is rather complicated, therefore, the corresponding analytic calculations of its surface Fermi states are quite involved and not much revealing. Therefore our general strategy in analyzing these states will be to start from a simplified model and then move forward to the realistic model by adding step-by-step the necessary missing pieces.

III. SURFACE FERMI ARCS IN SIMPLIFIED 2×2 MODEL

In order to get an insight into the structure of the surface Fermi arcs in the low-energy model described by Hamiltonian (1), it is instructive to first study the surface Fermi arcs in a simplified 2×2 model, given by one of the diagonal blocks, e.g., $H^{+}_{2\times2}$ in Eq. (10). (The solutions for the other block Hamiltonian, $H^{-}_{2\times2}$, can be obtained simply by changing $k_x \to -k_x$.) For completeness, we will also include the term $\epsilon_0(\mathbf{k})$ proportional to the unit matrix, which is present in the low-energy Hamiltonian. Thus our model 2×2 Hamiltonian reads

$$H_{2\times2} = \epsilon_0(\mathbf{k}) + H^{+}_{2\times2} = \epsilon_0(\mathbf{k}) + \begin{pmatrix} M_0 - M_1 k_z^2 - M_2\left(k_x^2 + k_y^2\right) & A(k_x + ik_y) \\ A(k_x - ik_y) & -\left[M_0 - M_1 k_z^2 - M_2\left(k_x^2 + k_y^2\right)\right] \end{pmatrix}. \tag{14}$$

Before proceeding to the analysis, it is convenient to perform a unitary transformation, $\tilde{H}_{2\times2} \equiv U_y^{-1} H_{2\times2} U_y$, where $U_y = \frac{1}{\sqrt{2}}(I_2 + i\sigma_y)$. The transformed Hamiltonian has the following explicit form:

$$\tilde{H}_{2\times2} = \epsilon_0(\mathbf{k}) + \left[\gamma\left(k_z^2 - m\right) - M_2\left(k_x^2 + k_y^2\right)\right]\sigma_x - v k_x \sigma_z - v k_y \sigma_y, \tag{15}$$

where we introduced the notations similar to those in Ref. [29]: $v = A$ and $\gamma = -M_1$.

To study the surface Fermi arcs, we will assume that the surface of a semimetal is at $y = 0$. The semimetal itself is in the upper $y > 0$ (lower $y < 0$) half-space when we describe the surface arc states on the bottom (top) surface. (Of course, in the absence of any effects that break the inversion symmetry $k_y \to -k_y$ explicitly, the two cases will be related by a simple symmetry transformation.) Without loss of generality, we will concentrate primarily on the bottom surface states. The boundary condition on the semimetal surface will be imposed by replacing the parameter m with the $-\tilde{m}$ on the vacuum side of the boundary and taking the limit $\tilde{m} \to \infty$ [29]. From a physics viewpoint, such a replacement is the simplest way to prevent quasiparticle from escaping into the vacuum.

Taking into account that the Fermi arc states should be localized at the $y = 0$ boundary, let us rewrite Hamiltonian (15) in the following form:

$$\tilde{H}_{2\times2} = \begin{pmatrix} C_0 + C_1 k_z^2 + C_2\left(k_x^2 - \partial_y^2\right) - v k_x & \gamma\left(k_z^2 - m\right) - M_2\left(k_x^2 - \partial_y^2\right) + v\partial_y \\ \gamma\left(k_z^2 - m\right) - M_2\left(k_x^2 - \partial_y^2\right) - v\partial_y & C_0 + C_1 k_z^2 + C_2\left(k_x^2 - \partial_y^2\right) + v k_x \end{pmatrix}, \tag{16}$$

where, for the convenience of further derivations, we replaced $k_y \equiv -i\partial_y$.

A. Simplified model with $C_2 = M_2 = 0$

We will see in what follows that the presence of the terms with the second derivative with respect to y in Hamiltonian (16) leads to many technical complications and makes the analysis rather involved. Therefore, to set up the stage, in this subsection we start our analysis in an even more simplified model, described by Hamiltonian (16) with C_2 and M_2 set to zero. Then, by introducing the two-component spinor $\Psi = (\psi_1, \psi_2)^T$, we see that the eigenvalue problem $(\tilde{H}_{2\times2} - E)\Psi = 0$ is equivalent to the following system of equations:

$$\left(-v k_x + C_1 k_z^2 + C_0\right)\psi_1 + \left[v\partial_y + \gamma k_z^2 - \gamma m(y)\right]\psi_2 = E\psi_1, \tag{17}$$

$$\left(v k_x + C_1 k_z^2 + C_0\right)\psi_2 + \left[-v\partial_y + \gamma k_z^2 - \gamma m(y)\right]\psi_1 = E\psi_2. \tag{18}$$

Here, $m(y) = m\theta(y) - \tilde{m}\theta(-y)$, where $\theta(y)$ is the step function. Recall that, by assumption, the boundary condition at $y = 0$ is enforced by taking the limit $\tilde{m} \to \infty$ on the vacuum side ($y < 0$). Formally, Eqs. (17) and (18) have the following surface state solutions:

$$\Psi_1(y) = \begin{pmatrix} N_1 e^{\frac{\gamma}{v}\int^y dy'[k_z^2 - m(y')]} \\ 0 \end{pmatrix},$$
$$\Psi_2(y) = \begin{pmatrix} 0 \\ N_2 e^{-\frac{\gamma}{v}\int^y dy'[k_z^2 - m(y')]} \end{pmatrix}. \quad (19)$$

In the region occupied by the semimetal ($y > 0$), the solution $\Psi_1(y)$ is normalizable only for $k_z^2 - m < 0$, while the solution $\Psi_2(y)$ is normalizable only for $k_z^2 - m > 0$. However, on the vacuum side ($y < 0$), only $\Psi_1(y)$ is normalizable. The dispersion relation for this normalizable surface state solution follows from Eq. (17). It is given by

$$E = -vk_x + C_1 k_z^2 + C_0. \quad (20)$$

By making use of this relation, we derive the equation for the bottom surface Fermi arc in the transverse $k_x k_z$ plane,

$$k_x = -\frac{E - C_1 k_z^2 - C_0}{v}. \quad (21)$$

It is instructive to compare this surface Fermi arc with that in the model of Ref. [29], where $C_1 = 0$. While the surface Fermi arcs run between $k_z = -\sqrt{m}$ and $k_z = \sqrt{m}$ in both models, the arcs in the model of Ref. [29] do not depend on the momentum k_z. This is in contrast to the surface Fermi arc in Eq. (21), for which k_x is a quadratic function of k_z. Thus we see that the presence of the quadratic in k_z term in the diagonal component of Hamiltonian (16) produces a nonzero *curvature* of the surface Fermi arcs in momentum space. For illustration, several surface Fermi arcs for different values of the Fermi energy are shown in Fig. 1. The arcs have parabolic shapes.

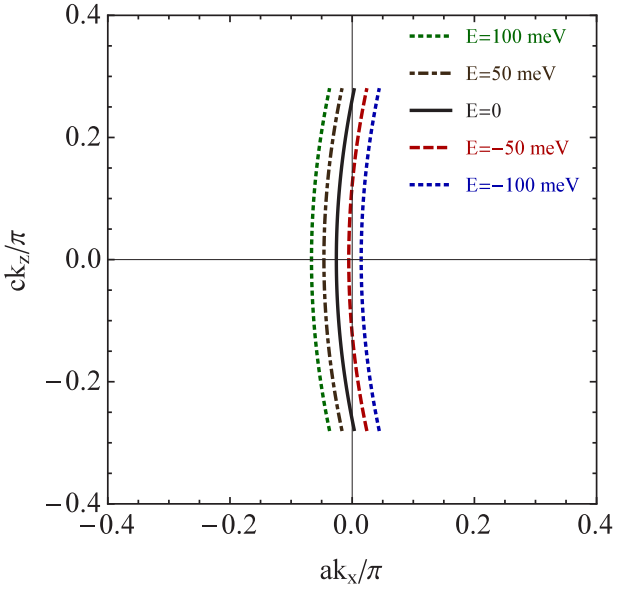

FIG. 1. (Color online) The bottom surface Fermi arcs for several different values of the Fermi energy in a simplified two-component model, described by Hamiltonian (16) with $C_2 = M_2 = 0$. The analytical form of the arcs is given in Eq. (21).

The corresponding arcs in the model of Ref. [29] would be given by straight lines.

Before concluding this section, let us note that the solution $\Psi_2(y)$ in Eq. (19) describes Fermi arcs on the top surface. We find from Eq. (18) that the corresponding dispersion relation is given by $E = vk_x + C_1 k_z^2 + C_0$. Let us also note in passing that there exists another set of the (top and bottom) Fermi arcs for the lower block Hamiltonian, $H_{2\times2}^-$. The corresponding arcs are obtained from the solutions for the upper block Hamiltonian, $H_{2\times2}^+$, by making the replacement $k_x \to -k_x$.

B. The case with $C_2 \neq 0$ and $M_2 \neq 0$

Let us now consider the general case with $C_2 \neq 0$ and $M_2 \neq 0$. By noting that the Hamiltonian in Eq. (16) contains second derivatives with respect to y, the eigenvalue problem $(\tilde{H}_{2\times2} - E)\Psi = 0$ becomes more complicated. In the semimetal ($y > 0$), it is equivalent to the following system of coupled equations:

$$\left[C_2\left(k_x^2 - \partial_y^2\right) - vk_x + C_1 k_z^2 + C_0\right]\psi_1 + \left[-M_2\left(k_x^2 - \partial_y^2\right) + v\partial_y + \gamma k_z^2 - \gamma m\right]\psi_2 = E\psi_1, \quad (22)$$

$$\left[C_2\left(k_x^2 - \partial_y^2\right) + vk_x + C_1 k_z^2 + C_0\right]\psi_2 + \left[-M_2\left(k_x^2 - \partial_y^2\right) - v\partial_y + \gamma k_z^2 - \gamma m\right]\psi_1 = E\psi_2. \quad (23)$$

On the vacuum side ($y < 0$), the corresponding set of equations has the same form, but with m replaced by $-\tilde{m}$. At the vacuum-semimetal interface ($y = 0$), the wave functions and their derivatives should satisfy the conditions of continuity, see Eqs. (A1) through (A4) in Appendix A1.

The key details of the derivation of the surface Fermi arc solutions are presented in Appendix A1. On the semimetal side, the spinor structure of the solution takes the following form:

$$\Psi_{y>0}(y) = \sum_{i=1}^{2} \begin{pmatrix} a_i \\ b_i \end{pmatrix} e^{-p_i y}, \quad (24)$$

where the explicit expressions for the exponents are given in Eq. (A9). Note that the exponents take real values in the case of surface Fermi arc states. The condition of existence of nontrivial surface Fermi arc solutions is given by

$$\frac{-C_2\left(p_1^2 - k_x^2\right) + C_1 k_z^2 + C_0 - E - vk_x}{-M_2\left(p_1^2 - k_x^2\right) - \gamma\left(k_z^2 - m\right) + vp_1} = \frac{-C_2\left(p_2^2 - k_x^2\right) + C_1 k_z^2 + C_0 - E - vk_x}{-M_2\left(p_2^2 - k_x^2\right) - \gamma\left(k_z^2 - m\right) + vp_2}. \quad (25)$$

This equation defines the functional dependence $k_z(k_x)$ for the possible surface Fermi arc states. A numerical study shows that nontrivial solutions exist only in a finite range of energies, i.e., $-0.168\ \text{eV} \lesssim E \lesssim 0.373\ \text{eV}$. Several solutions for different values of the energy are shown in Fig. 2. The results of the numerical analysis show that the following condition is satisfied: $b_1/a_1 = b_2/a_2 = 0.5115$ for all solutions. It is worth noting that the $E = 0$ surface Fermi arc in Fig. 2 appears to be almost identical to the corresponding arc, obtained by a very different method in Ref. [4], see Fig. 3(c) in that paper.

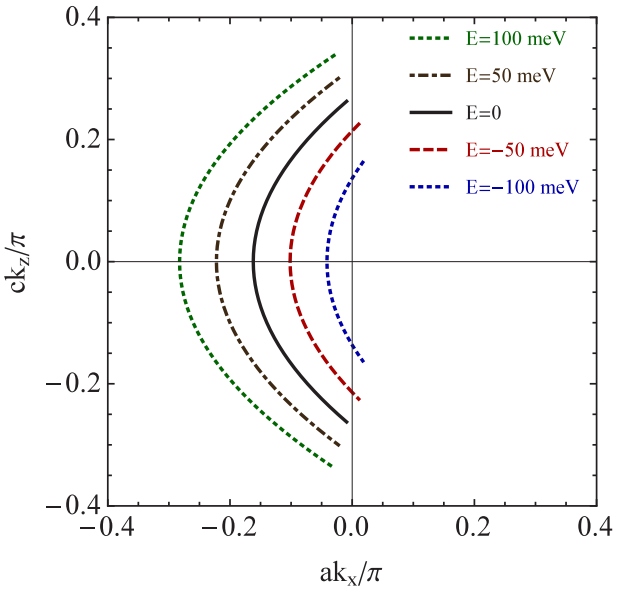

FIG. 2. (Color online) The bottom surface Fermi arcs (25) for several values of the Fermi energy in a two-component model, described by Hamiltonian (16) with $C_2 \neq 0$ and $M_2 \neq 0$.

So far, we considered the arc states only for one of the two-component block Hamiltonians, defined in Eq. (14). Similar solutions also exist for the lower two-component block Hamiltonian, $\epsilon_0(\mathbf{k}) + H^-_{2\times2}$. It is straightforward to show that the solutions to the eigenvalue problem for the lower block are the same as for the upper one, after one makes the replacement $k_x \to -k_x$. Graphically, these solutions are mirror images of the arcs in Fig. 2.

Before concluding this subsection, let us also note that the description of the Fermi arc states on the top surface is similar to the bottom ones. By assuming that Weyl semimetal is at $y < 0$ and the vacuum is at $y > 0$, the appropriate boundary conditions are implemented by using the y-dependent parameter $m(y) = m\theta(-y) - \tilde{m}\theta(y)$ and taking the limit $\tilde{m} \to \infty$ at the end. Up to a reflection $k_x \to -k_x$, the corresponding final results for the Fermi arcs on the top surface look similar to those on the bottom surface, shown in Fig. 2.

C. Effective Hamiltonian for surface Fermi arc states

Following the usual approach in the studies of topological insulator [35], it may be natural to derive an effective Hamiltonian for the surface Fermi arc states. The block Hamiltonians in the simplified model at hand can be naturally separated into two parts, i.e., $\tilde{H}^{\pm}_{2\times2} = H_0 + H^{\pm}_1$, where the zeroth order part H_0 corresponds to the original Hamiltonian at $k_x = k_z = 0$, i.e.,

$$H_0 = \begin{pmatrix} C_0 - C_2\partial_y^2 & -\gamma m + M_2\partial_y^2 + v\partial_y \\ -\gamma m + M_2\partial_y^2 - v\partial_y & C_0 - C_2\partial_y^2 \end{pmatrix}. \quad (26)$$

while H_1 contains all the terms with nontrivial dependence on k_x and k_z, i.e.,

$$H_1^{\pm} = \begin{pmatrix} C_1k_z^2 + C_2k_x^2 \mp vk_x & \gamma k_z^2 - M_2k_x^2 \\ \gamma k_z^2 - M_2k_x^2 & C_1k_z^2 + C_2k_x^2 \pm vk_x \end{pmatrix}. \quad (27)$$

As in the previous analysis, we used $k_y \equiv -i\partial_y$. To start with, we have to solve the eigenvalue problem with the zeroth order Hamiltonian, $H_0\Psi_0 = \lambda\Psi_0$. By following the same approach as in Appendix A1, but with $k_x = k_z = 0$, we find straightforwardly the explicit solutions for the surface Fermi arcs Ψ_0. The corresponding energy parameter is found to be $\lambda = -0.13425$ eV. Then, the effective Hamiltonian for the surface states is obtained by integrating over the perpendicular direction y, i.e.,

$$\begin{aligned} H^{\pm}_{\rm surf} &= \lambda + \int_0^\infty dy\,\Psi_0^\dagger H_1\Psi_0 = \lambda + C_1k_z^2 + C_2k_x^2 \\ &\quad \mp vk_x\frac{1-Q^2}{1+Q^2} + 2\big(\gamma k_z^2 - M_2k_x^2\big)\frac{Q}{1+Q^2} \\ &\approx \lambda \mp v_{\rm surf}k_x + \gamma_{\rm surf}k_z^2. \end{aligned} \quad (28)$$

where $Q \approx 0.5115$, $v_{\rm surf} \approx 1.440$ eV Å, and $\gamma_{\rm surf} \approx 17.38$ eV Å^2. Note that the quadratic term in k_x vanishes after the model parameters are used.

As is easy to check, the effective Hamiltonian in Eq. (28) reproduces almost perfectly the shape of the Fermi arcs in the k_xk_z plane. However, it does not contain the information about the finite length of the arcs. We could explain this fact in part by pointing out that the corresponding information is encoded in the terms quadratic in momenta k_x and k_z. When such terms are omitted from the zeroth order Hamiltonian H_0, the existence of the surface states formally appears to be unconstrained. Therefore the effective Hamiltonian in Eq. (28) will be truly useful only when supplemented by its range of validity in the k_xk_z plane. This, however, seems to diminish its practical value because the corresponding range depends on the energy.

IV. FERMI ARCS IN REALISTIC MODEL

In this section, we will consider the complete low-energy theory described by Hamiltonian (1) with $\alpha \neq 0$. By performing a unitary transformation in Eq. (1), defined by $U_y = \frac{1}{\sqrt{2}}I_2 \otimes (I_2 + i\sigma_y)$, we arrive at the following equivalent form of the Hamiltonian:

$$\begin{aligned} \tilde{H} &= \big[C_2\big(k_x^2 - \partial_y^2\big) + C_1k_z^2 + C_0\big]I_2 \otimes I_2 - M_2\big(k_x^2 - \partial_y^2\big)I_2 \otimes \sigma_x \\ &\quad + \begin{pmatrix} -vk_x & v\partial_y + \gamma\big(k_z^2 - m\big) & -\alpha k_z(k_x - \partial_y)^2 & 0 \\ -v\partial_y + \gamma\big(k_z^2 - m\big) & vk_x & 0 & \alpha k_z(k_x - \partial_y)^2 \\ -\alpha k_z(k_x + \partial_y)^2 & 0 & vk_x & v\partial_y + \gamma\big(k_z^2 - m\big) \\ 0 & \alpha k_z(k_x + \partial_y)^2 & -v\partial_y + \gamma\big(k_z^2 - m\big) & -vk_x \end{pmatrix}, \end{aligned} \quad (29)$$

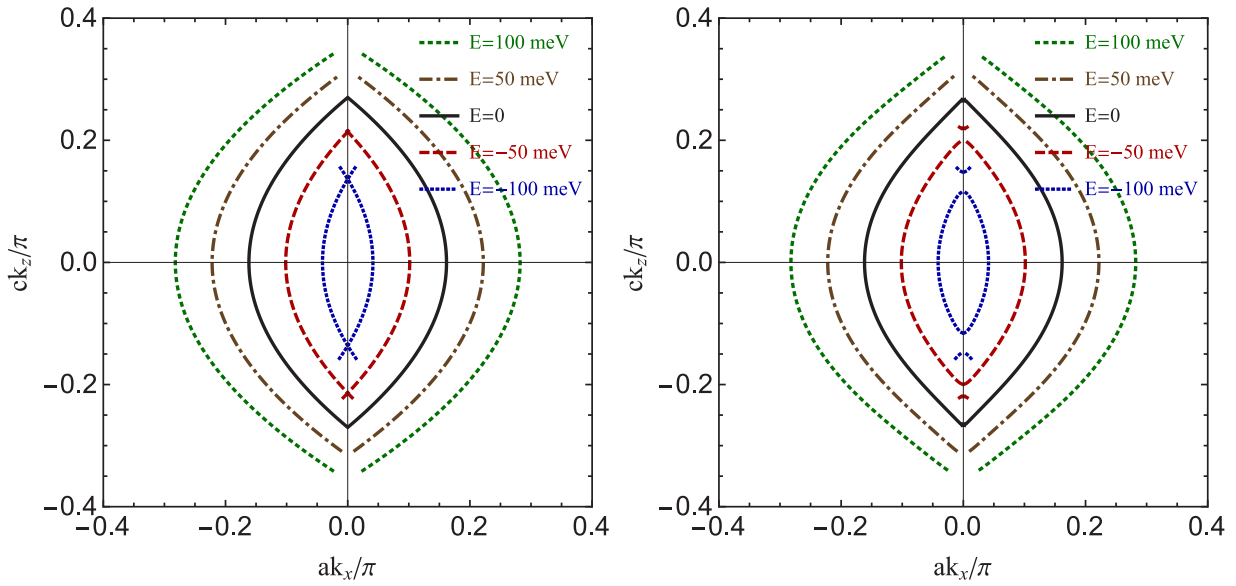

FIG. 3. (Color online) The Fermi arcs solutions in the plane of transverse momenta for $\alpha = 1$ eV Å^3 (left) and $\alpha = 50$ eV Å^3 (right).

By introducing the spinor wave function $\Psi = (\psi_1, \psi_2, \psi_3, \psi_4)^T$, we reduce the eigenvalue problem $(\tilde{H} - E)\Psi = 0$ in the semimetal ($y > 0$) to the following system of equations:

$$\left[C_2\left(k_x^2 - \partial_y^2\right) - vk_x + C_1 k_z^2 + C_0 - E\right]\psi_1 + \left[-M_2\left(k_x^2 - \partial_y^2\right) + v\partial_y + \gamma k_z^2 - \gamma m\right]\psi_2 - \alpha k_z(k_x - \partial_y)^2\psi_3 = 0, \quad (30)$$

$$\left[-M_2\left(k_x^2 - \partial_y^2\right) - v\partial_y + \gamma k_z^2 - \gamma m\right]\psi_1 + \left[C_2\left(k_x^2 - \partial_y^2\right) + vk_x + C_1 k_z^2 + C_0 - E\right]\psi_2 + \alpha k_z(k_x - \partial_y)^2\psi_4 = 0, \quad (31)$$

$$-\alpha k_z(k_x + \partial_y)^2\psi_1 + \left[C_2\left(k_x^2 - \partial_y^2\right) + vk_x + C_1 k_z^2 + C_0 - E\right]\psi_3 + \left[-M_2\left(k_x^2 - \partial_y^2\right) + v\partial_y + \gamma k_z^2 - \gamma m\right]\psi_4 = 0, \quad (32)$$

$$\alpha k_z(k_x + \partial_y)^2\psi_2 + \left[-M_2\left(k_x^2 - \partial_y^2\right) - v\partial_y + \gamma k_z^2 - \gamma m\right]\psi_3 + \left[C_2\left(k_x^2 - \partial_y^2\right) - vk_x + C_1 k_z^2 + C_0 - E\right]\psi_4 = 0. \quad (33)$$

On the vacuum side ($y < 0$), the corresponding set of equations has the same form, but with m replaced by $-\tilde{m}$. The corresponding full set of equations should be also supplemented by the conditions of continuity of the wave functions and their derivatives across the vacuum-semimetal interface at $y = 0$, see Eqs. (A16) through (A20) in Appendix A2.

As shown in Appendix A2, the spinor structure of the solution on the semimetal side takes the form

$$\Psi_{y>0}(y) = \sum_{i=1}^{2} \begin{pmatrix} a_i \\ b_i \\ c_i \\ d_i \end{pmatrix} e^{-p_i y}, \quad (34)$$

where the explicit expressions for the exponents are given in Eq. (A23). In the case of surface Fermi arc solutions, the exponents take real values. A nontrivial solution exists when the following condition is satisfied:

$$(Q_1^+ - Q_2^+)(Q_1^- - Q_2^-) - (T_1^+ - T_2^+)(T_1^- - T_2^-) = 0, \quad (35)$$

where, by definition, $Q_i^{\pm} \equiv Q(p_i, \pm k_x)$ and $T_i^{\pm} \equiv T(p_i, \pm k_x)$, and the functions $Q(p, k_x)$ and $T(p, k_x)$ are defined in Eqs. (A12) and (A26), respectively.

By taking into account that $T(p, k_x)$ vanishes at $\alpha = 0$, one finds that the above condition reduces to its analog in Eq. (25) in the two-component model. Indeed, a nontrivial solution exists in the model with the two-component upper (lower) block Hamiltonian when $Q_1^+ = Q_2^+$ ($Q_1^- = Q_2^-$) is satisfied. We would like to emphasize that the classification of the arc states remains essentially the same also in a general case with $\alpha \neq 0$. However, because of the mixing between the upper and lower block Hamiltonians, the arcs are labeled by the eigenvalues of the U_χ operator, see Appendix B. The eigenstates with $\chi = +1$ ($\chi = -1$) are the generalizations of the arcs from the upper (lower) block Hamiltonian.

The numerical results for the surface Fermi arc states are shown in Fig. 3 for $\alpha = 1$ eV Å^3 (left panel) and $\alpha = 50$ eV Å^3 (right panel). At fixed energy, there are two surface Fermi arcs related to two different sectors of the A_3Bi (A = Na,K,Rb) compounds with definite eigenvalue of U_χ. One can check that the wave functions that describe these surface Fermi arcs are related to each other by means of the $\tilde{U}\Pi_{k_x}$ transformation, see Appendix B. By comparing these results with those in the two-component model, see Fig. 2, we find that the quantitative effect of a nonzero α on the Fermi arcs is small even when α is moderately large. The only qualitative effect due to α is a reconnection of the pair of arcs (from predominantly up and predominantly down sectors) at negative values of the Fermi energy. The underlying physics of such an effect is likely to be connected with the loss of the chirality as a good quantum number for quasiparticles away from the Dirac/Weyl nodes. Because of the discrete ud-parity, which is preserved even at large values of α, there are still two sectors of the theory and there are still small nontrivial arcs present, as we see from the right panel of Fig. 3. It will be interesting to explore whether

the reconnection of the pairs of arcs would also appear in the microscopic theory. It may well be an artifact of the low-energy theory used here.

V. FERMI ARCS AND WEAK BREAKING OF TIME-REVERSAL SYMMETRY

As we discussed in detail in Sec. II B, the low-energy effective Hamiltonian (1) is invariant under the time-reversal and inversion symmetries. Moreover, these symmetries play an important role in defining the physical properties of A_3Bi semimetals. Thus it is natural to ask about possible effects on the structure (and perhaps even the existence) of surface Fermi arcs due to breaking of these symmetries. From the physics viewpoint, for example, the corresponding discrete symmetries could be broken explicitly by magnetic doping or an external magnetic field.

In order to study the symmetry breaking effects, we will add to the low-energy Hamiltonian (1) two additional terms controlled by parameters m_1 and $\tilde{\mu}_1$:

$$H_{\rm sb} = H(\mathbf{k}) - \begin{pmatrix} \tilde{\mu}_1 I_2 + \sigma_z \gamma m_1 & 0 \\ 0 & -\tilde{\mu}_1 I_2 - \sigma_z \gamma m_1 \end{pmatrix}. \quad (36)$$

By analyzing the Schwinger-Dyson equation for the quasiparticle propagator in A_3Bi semimetals in a magnetic field, we found that these terms are indeed perturbatively generated. Alternatively, these terms can be induced by magnetic doping. The value of $\tilde{\mu}_1$ could be interpreted as a mismatch between the chemical potentials of quasiparticle states in the Weyl sectors of the theory. The value of m_1 is a mismatch of the parameter m that determines the chiral shift in the two sectors. This means that whenever these symmetry breaking parameters appear, the $\mathbb{Z}_2$ Weyl semimetal will get automatically transformed into a true Weyl semimetal with four nondegenerate Weyl nodes.

By performing a unitary transformation in Eq. (36), defined by matrix $U_y = \frac{1}{\sqrt{2}} I_2 \otimes (I_2 + i\sigma_y)$, we arrive at the following equivalent Hamiltonian:

$$\tilde{H}_{\rm sb} = \left[C_2\left(k_x^2 - \partial_y^2\right) + C_1 k_z^2 + C_0\right] I_2 \otimes I_2 - M_2\left(k_x^2 - \partial_y^2\right) I_2 \otimes \sigma_x + \begin{pmatrix} -vk_x - \tilde{\mu}_1 & v\partial_y + \gamma\left(k_z^2 - m - m_1\right) & -\alpha k_z (k_x - \partial_y)^2 & 0 \\ -v\partial_y + \gamma\left(k_z^2 - m - m_1\right) & vk_x - \tilde{\mu}_1 & 0 & \alpha k_z (k_x - \partial_y)^2 \\ -\alpha k_z (k_x + \partial_y)^2 & 0 & vk_x + \tilde{\mu}_1 & v\partial_y + \gamma\left(k_z^2 - m + m_1\right) \\ 0 & \alpha k_z (k_x + \partial_y)^2 & -v\partial_y + \gamma\left(k_z^2 - m + m_1\right) & -vk_x + \tilde{\mu}_1 \end{pmatrix}. \quad (37)$$

It is straightforward, although tedious to repeat the same analysis as in Sec. IV.

The general surface state solution is of the same type, i.e., $\Psi_{y>0}(y) = \Psi_0 e^{-py}$, where $\Psi_0 \equiv (a,b,c,d)^T$ is a constant spinor. However, the characteristic equation is considerably more complicated,

$$\begin{aligned} &\left\{\left[-C_2\left(p^2 - k_x^2\right) + C_1 k_z^2 + C_0 - \tilde{\mu}_1 - E\right]^2 - \left[M_2\left(p^2 - k_x^2\right) + \gamma\left(k_z^2 - m - m_1\right)\right]^2 + v^2\left(p^2 - k_x^2\right) - \alpha^2 k_z^2 \left(p^2 - k_x^2\right)^2\right\} \\ &\times \left\{\left[-C_2\left(p^2 - k_x^2\right) + C_1 k_z^2 + C_0 + \tilde{\mu}_1 - E\right]^2 - \left[M_2\left(p^2 - k_x^2\right) + \gamma\left(k_z^2 - m + m_1\right)\right]^2 + v^2\left(p^2 - k_x^2\right) - \alpha^2 k_z^2 \left(p^2 - k_x^2\right)^2\right\} \\ &+ 4\alpha^2 k_z^2 \left(p^2 - k_x^2\right)^2 \left(\tilde{\mu}_1^2 - \gamma^2 m_1^2\right) = 0. \end{aligned} \quad (38)$$

The important effect of the symmetry breaking terms with nonzero m_1 and $\tilde{\mu}_1$ is that the new characteristic equation has *four* (instead of two degenerate) pairs of distinct solutions: $p = \pm p_i$, with $i = 1,2,3,4$. The general spinor solution in the semimetal takes the following form:

$$\Psi_{y>0}(y) = \sum_{i=1}^{4} \begin{pmatrix} a_i \\ b_i \\ c_i \\ d_i \end{pmatrix} e^{-p_i y}. \quad (39)$$

By making use of the equation of motion, the components b_i and d_i can be expressed in terms of a_i and c_i,

$$b_i = \frac{-C_2\left(p_i^2 - k_x^2\right) + C_1 k_z^2 + C_0 - \tilde{\mu}_1 - E - vk_x}{-M_2\left(p_i^2 - k_x^2\right) - \gamma\left(k_z^2 - m - m_1\right) + vp_i} a_i - \frac{\alpha k_z (p_i + k_x)^2}{-M_2\left(p_i^2 - k_x^2\right) - \gamma\left(k_z^2 - m - m_1\right) + vp_i} c_i, \quad (40)$$

$$d_i = -\frac{\alpha k_z (p_i - k_x)^2}{-M_2\left(p_i^2 - k_x^2\right) - \gamma\left(k_z^2 - m + m_1\right) + vp_i} a_i + \frac{-C_2\left(p_i^2 - k_x^2\right) + C_1 k_z^2 + C_0 + \tilde{\mu}_1 - E - vk_x}{-M_2\left(p_i^2 - k_x^2\right) - \gamma\left(k_z^2 - m + m_1\right) + vp_i} c_i. \quad (41)$$

In order to avoid a possible confusion, let us emphasize that the remaining two components a_i and c_i are not independent, but fixed unambiguously for each p_i. The final solutions for the Fermi arcs are determined after all four independent parameters (e.g., a_i with $i = 1,2,3,4$) are fixed by satisfying the continuity conditions for the wave function at the surface of the semimetal. The corresponding solutions can be obtained by numerical methods.

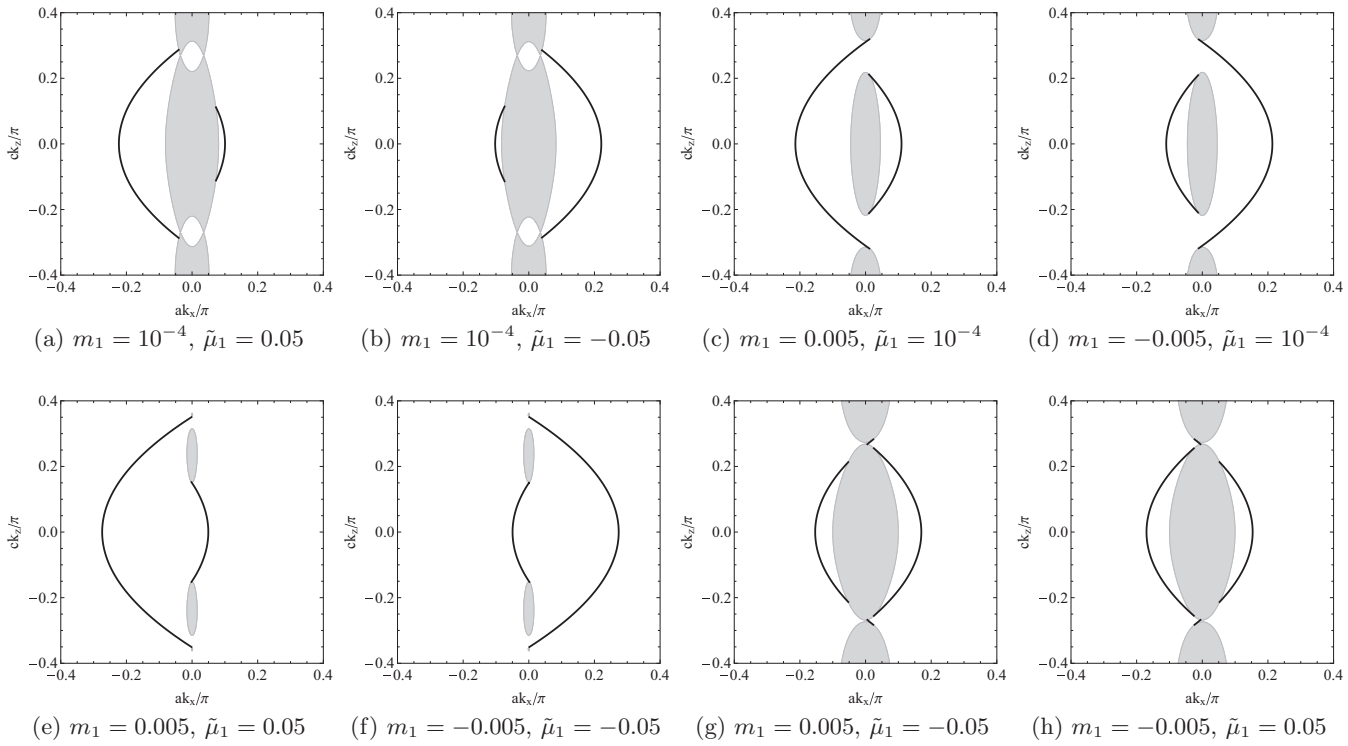

(a) $m_1 = 10^{-4}$, $\tilde{\mu}_1 = 0.05$ (b) $m_1 = 10^{-4}$, $\tilde{\mu}_1 = -0.05$ (c) $m_1 = 0.005$, $\tilde{\mu}_1 = 10^{-4}$ (d) $m_1 = -0.005$, $\tilde{\mu}_1 = 10^{-4}$

(e) $m_1 = 0.005$, $\tilde{\mu}_1 = 0.05$ (f) $m_1 = -0.005$, $\tilde{\mu}_1 = -0.05$ (g) $m_1 = 0.005$, $\tilde{\mu}_1 = -0.05$ (h) $m_1 = -0.005$, $\tilde{\mu}_1 = 0.05$

FIG. 4. The Fermi arcs solutions (thick black lines) in the model with the symmetry breaking parameters m_1 and $\tilde{\mu}_1$ at $E = 0$. The shaded regions represent the projections of the bulk Fermi surfaces onto the $k_x k_z$ plane. The values of m_1 and $\tilde{\mu}_1$ are given in units of Å^{-2} and eV, respectively.

To slightly simplify the analysis, let us consider a special case of vanishing α in more detail. In this case, the states from the two-component upper and lower block Hamiltonians decouple. Also, the characteristic equation factorizes, effectively giving two separate equations, i.e.,

$$\left[-C_2\left(p^2 - k_x^2\right) + C_1 k_z^2 + C_0 - \tilde{\mu}_1 - E\right]^2 - \left[M_2\left(p^2 - k_x^2\right) + \gamma\left(k_z^2 - m - m_1\right)\right]^2 + v^2\left(p^2 - k_x^2\right) = 0 \quad \text{(up)}, \tag{42}$$

$$\left[-C_2\left(p^2 - k_x^2\right) + C_1 k_z^2 + C_0 + \tilde{\mu}_1 - E\right]^2 - \left[M_2\left(p^2 - k_x^2\right) + \gamma\left(k_z^2 - m + m_1\right)\right]^2 + v^2\left(p^2 - k_x^2\right) = 0 \quad \text{(down)}, \tag{43}$$

cf. Eq. (A8). Then, the analysis of the surface Fermi arcs follows very closely the analysis in Sec. III B.

A number of representative numerical solutions for the Fermi surface arcs in the model with the symmetry breaking parameters m_1 and $\tilde{\mu}_1$ are shown in Fig. 4. The results are obtained for the Fermi energy $E = 0$. In order to shed light on the origin of the individual arcs, in the same figure we also show the projections (shaded regions) of the bulk Fermi surfaces onto the $k_x k_z$ plane. Such a representation reveals that some of the Fermi arcs link *disconnected* sheets of the bulk Fermi surface [27], while others link different points of the *same* bulk Fermi surface sheet.

As suggested by the physical meaning of the symmetry breaking parameters, m_1 and $\tilde{\mu}_1$, the Fermi surface arcs for the up and down Weyl sectors of the theory are not transformed into each other by a mirror symmetry. In addition to the expected effects of (i) changing the length of the arcs (primarily due to nonzero m_1) and (ii) shifting the arcs' position in the k_x direction (primarily due to nonzero $\tilde{\mu}_1$), we also see some qualitative changes in the shape and branching of the arcs. By comparing Eqs. (42) and (43) for the two sectors of the theory, we find that the whole asymmetric sets of the Fermi arcs turn into their mirror reflections when both parameters m_1 and $\tilde{\mu}_1$ change their signs. Examples of two pairs of such mirror configurations are shown in panels (e)–(f) and (g)–(h) in Fig. 4. [Strictly speaking, the other two pairs of configurations, see (a)–(b) and (c)–(d), are not exact mirror reflections of each other because one of the symmetry breaking parameters does not change the sign. Because of a smallness of the parameter, there is an appearance of approximate mirror configurations.]

It is interesting to point out that different topologies of the global (bulk-plus-arcs) Fermi hypersurfaces, including the bulk sheets and the surface Fermi arcs, are possible. For example, for a range of symmetry breaking parameters, represented by panels (c), (d), (e), and (f) in Fig. 4, we find that the global Fermi hypersurfaces consist of pairs of clearly disconnected parts. This is in contrast to the configurations in panels (a) and (b), where different parts touch at four points, and in contrast to the configurations in panels (g) and (h), where all parts of the global Fermi hypersurfaces are linked

by the Fermi arcs. If samples with completely disconnected parts of the global Fermi hypersurfaces are indeed possible, they will be very interesting to study in experiments.

As we see from panels (g) and (h) in Fig. 4, there are also qualitatively new types of the Fermi arcs possible for a range of symmetry breaking parameters. In particular, we find a pair of "short" branches of the Fermi arcs that split off from the usual "long" arcs. To the best of our knowledge, the corresponding short arcs have not been predicted before. So far, we could not establish a general criterion for the existence of the short arcs. In the configurations in panels (g) and (h), they play a profound role by linking two disconnected sheets of the bulk Fermi surface.

VI. CONCLUSION

In this paper, we studied the surface Fermi arc states by employing a continuum low-energy effective model. The use of analytical methods and a realistic low-energy model provide a deeper insight into the physical properties and characteristics of the surface Fermi arcs. In particular, we were able to classify the Fermi arcs with respect to the ud-parity and reconfirm the $\mathbb{Z}_2$ Weyl structure of A_3Bi semimetals [33]. In this context, it should be noted that the experimental observation of the corresponding Fermi arc states have been recently reported for Na_3Bi [36]. While in agreement with the claimed topological semimetal structure, such an observation does not confirm it unambiguously. That is because the Fermi arc states are also possible in Dirac materials where the $\mathbb{Z}_2$ Weyl structure is absent [5,31]. The unambiguous confirmation of the $\mathbb{Z}_2$ Weyl structure could, however, be established via the quantum oscillations, whose period should dependent on the thickness of the semimetal in the same way as in true Weyl semimetals [31,32].

By introducing the effects of several possible symmetry breaking terms, we show that the $\mathbb{Z}_2$ Weyl structure of A_3Bi is destroyed in a very special way: the compounds become true Weyl semimetals. We suggest that this finding can be tested in experiment. For example, by taking into account that the mirror-symmetric pairs of surface Fermi arcs in clean A_3Bi get distorted upon the introduction of explicit symmetry breaking (e.g., by magnetic doping), a number of specific features (size, shape and number of branches) should be seen in the surface Fermi arcs. The corresponding properties could be studied, for example, by analyzing the quantum oscillations sensitive to the surface states of this type [31]. In the absence of symmetry breaking, there will be a unique period of oscillations dependent in a specific way on the thickness of the semimetal slab [32]. On the other hand, the breaking of symmetry will produce pairs of inequivalent arcs of different lengths and the observation of two incommensurate periods of oscillations will be expected. In principle, by making use of the analytical results in this study, the details of the oscillations could be used to estimate the magnitude of the symmetry breaking terms.

ACKNOWLEDGMENTS

The work of E.V.G. was supported partially by the Ukrainian State Foundation for Fundamental Research. The work of V.A.M. was supported by the Natural Sciences and Engineering Research Council of Canada. The work of I.A.S. was supported by the U.S. National Science Foundation under Grant No. PHY-1404232.

APPENDIX A: DERIVATIONS OF SURFACE FERMI ARCS SOLUTIONS

In this appendix, we present the key technical details of deriving the surface Fermi arcs solutions in the 2×2 model, introduced in Sec. III B, and in the 4×4 model, introduced in Sec. IV.

1. Surface Fermi arcs in 2×2 model

Let us start with the analysis of the surface Fermi arc states in the 2×2 model, introduced in Sec. III B. The problem reduces to solving the eigenvalues problem given by Eqs. (22) and (23) at $y > 0$ (semimetal), as well as a similar set of equations at $y < 0$ (vacuum), but m replaced by $-\tilde{m}$. The corresponding set of equations should be also supplemented by the boundary conditions at the vacuum-semimetal interface, i.e.,

$$\tilde{\psi}_1(-0) = \psi_1(+0), \tag{A1}$$

$$\tilde{\psi}_2(-0) = \psi_2(+0), \tag{A2}$$

$$-C_2\partial_y\tilde{\psi}_1(-0) + M_2\partial_y\tilde{\psi}_2(-0) = -C_2\partial_y\psi_1(+0) + M_2\partial_y\psi_2(+0), \tag{A3}$$

$$-M_2\partial_y\tilde{\psi}_1(-0) + C_2\partial_y\tilde{\psi}_2(-0) = -M_2\partial_y\psi_1(+0) + C_2\partial_y\psi_2(+0), \tag{A4}$$

where $\tilde{\psi}_{1,2}(y)$ correspond to the vacuum region at $y < 0$.

Inside the semimetal ($y > 0$), the surface state solutions should have the following form:

$$\Psi_{y>0}(y) = \begin{pmatrix} a \\ b \end{pmatrix} e^{-py}. \tag{A5}$$

By substituting this ansatz in Eqs. (22) and (23), we arrive at the following set of linear equations for the spinor components a and b:

$$\left[C_2\left(k_x^2 - p^2\right) - vk_x + C_1k_z^2 + C_0 - E\right]a + \left[-M_2\left(k_x^2 - p^2\right) - vp + \gamma k_z^2 - \gamma m\right]b = 0, \tag{A6}$$

$$\left[-M_2\left(k_x^2 - p^2\right) + vp + \gamma k_z^2 - \gamma m\right]a + \left[C_2\left(k_x^2 - p^2\right) + vk_x + C_1k_z^2 + C_0 - E\right]b = 0. \tag{A7}$$

A nontrivial solution exists when the following characteristic equation is satisfied:

$$\left[-C_2\left(p^2 - k_x^2\right) + C_1k_z^2 + C_0 - E\right]^2 - \left[M_2\left(p^2 - k_x^2\right) + \gamma k_z^2 - \gamma m\right]^2 + v^2\left(p^2 - k_x^2\right) = 0. \tag{A8}$$

The solutions to this equation are $p = \pm p_1$ and $p = \pm p_2$, where

$$p_1 = \sqrt{k_x^2 - \frac{X + \sqrt{X^2 + Y}}{2(M_2^2 - C_2^2)}},$$
$$p_2 = \sqrt{k_x^2 - \frac{X - \sqrt{X^2 + Y}}{2(M_2^2 - C_2^2)}}. \quad \text{(A9)}$$

Here, we introduced the following shorthand notations:

$$X \equiv 2C_2\left(C_1 k_z^2 + C_0 - E\right) + 2\gamma M_2\left(k_z^2 - m\right) - v^2, \quad \text{(A10)}$$

$$Y \equiv 4\left(M_2^2 - C_2^2\right)\left[\left(C_1 k_z^2 + C_0 - E\right)^2 - \gamma^2\left(k_z^2 - m\right)^2\right]. \quad \text{(A11)}$$

The spinor components a and b of the corresponding nontrivial solution satisfy the constraint

$$\frac{b}{a} = Q(p,k_x) \equiv \frac{-C_2\left(p^2 - k_x^2\right) + C_1 k_z^2 + C_0 - E - v k_x}{-M_2\left(p^2 - k_x^2\right) - \gamma\left(k_z^2 - m\right) + v p}. \quad \text{(A12)}$$

Inside the semimetal ($y > 0$), the wave function should fall off with increasing y. Thus we use only the negative exponents in the general solution, i.e.,

$$\Psi_{y>0}(y) \simeq a_1 \begin{pmatrix} 1 \\ Q_1 \end{pmatrix} e^{-p_1 y} + a_2 \begin{pmatrix} 1 \\ Q_2 \end{pmatrix} e^{-p_2 y}, \quad \text{(A13)}$$

where $Q_i \equiv Q(p_i,k_x)$ with $i = 1,2$.

In order to find the vacuum solution ($y < 0$), we replace $m \to -\tilde{m}$ and take the limit $\tilde{m} \to \infty$. This leads to the following general solution on the vacuum side:

$$\Psi_{y<0}(y) \simeq \frac{\tilde{a}_1}{\sqrt{\gamma\tilde{m}}} \begin{pmatrix} 1 \\ -1 \end{pmatrix} e^{\tilde{p}_1 y} + \frac{\tilde{a}_2}{\sqrt{\gamma\tilde{m}}} \begin{pmatrix} 1 \\ 1 \end{pmatrix} e^{\tilde{p}_2 y}, \quad \text{(A14)}$$

where, for convenience, we took the overall constants to be inversely proportional to $\sqrt{\gamma\tilde{m}}$. The exponents in the vacuum solution are determined by

$$\tilde{p}_1 \simeq \sqrt{\frac{\gamma\tilde{m}}{-M_2 - C_2}}, \quad \tilde{p}_2 \simeq \sqrt{\frac{\gamma\tilde{m}}{-M_2 + C_2}}. \quad \text{(A15)}$$

It is interesting to note that the conditions of the wave function continuity, see Eqs. (A1) and (A2), are the only important conditions to be satisfied. Indeed, the nontrivial solution of Eq. (A1) in the limit $\tilde{m} \to \infty$ implies that $a_1 = -a_2 \neq 0$. This is consistent with Eq. (A2) only when $Q_1 = Q_2$. Concerning the remaining boundary conditions in Eqs. (A3) and (A4), enforcing the continuity of the wave function derivative, they do not add any additional constraints. In fact, they are needed only for determining the vacuum spinor components $\tilde{a}_1$ and $\tilde{a}_2$ in terms of the nontrivial components a_1 and a_2 in the semimetal. Such (finite) solutions always exist. However, as is clear from Eq. (A14), the vacuum solution have no much physical content because it vanishes in the limit $\tilde{m} \to \infty$.

In conclusion, the boundary conditions at $y = 0$ are satisfied and, therefore, a nontrivial solution exists when $Q_1 = Q_2$. The explicit form of the corresponding condition is given in Eq. (25) in the main text.

2. Surface Fermi arcs in 4×4 model

The analysis of the realistic 4×4 model introduced in Sec. IV is slightly more involved, but qualitatively similar. The eigenvalues problem in this case is given by Eqs. (30) through (33) at $y > 0$ (semimetal), as well as a similar set of equations at $y < 0$ (vacuum), but with m replaced by $-\tilde{m}$. The conditions of continuity of the wave functions and their derivatives across the vacuum-semimetal surface at $y = 0$ are given by

$$\tilde{\psi}_i(-0) = \psi_i(+0), \quad \text{for} \quad i = 1,2,3,4, \quad \text{(A16)}$$

$$-C_2\partial_y\tilde{\psi}_1(-0) + M_2\partial_y\tilde{\psi}_2(-0) - \alpha k_z\partial_y\tilde{\psi}_3(-0) = -C_2\partial_y\psi_1(+0) + M_2\partial_y\psi_2(+0) - \alpha k_z\partial_y\psi_3(+0), \quad \text{(A17)}$$

$$M_2\partial_y\tilde{\psi}_1(-0) - C_2\partial_y\tilde{\psi}_2(-0) + \alpha k_z\partial_y\tilde{\psi}_4(-0) = M_2\partial_y\psi_1(+0) - C_2\partial_y\psi_2(+0) + \alpha k_z\partial_y\psi_4(+0), \quad \text{(A18)}$$

$$-\alpha k_z\partial_y\tilde{\psi}_1(-0) - C_2\partial_y\tilde{\psi}_3(-0) + M_2\partial_y\tilde{\psi}_4(-0) = -\alpha k_z\partial_y\psi_1(+0) - C_2\partial_y\psi_3(+0) + M_2\partial_y\psi_4(+0), \quad \text{(A19)}$$

$$\alpha k_z\partial_y\tilde{\psi}_2(-0) + M_2\partial_y\tilde{\psi}_3(-0) - C_2\partial_y\tilde{\psi}_4(-0) = \alpha k_z\partial_y\psi_2(+0) + M_2\partial_y\psi_3(+0) - C_2\partial_y\psi_4(+0). \quad \text{(A20)}$$

In the semimetal ($y > 0$), we look for a general surface state solution in the form

$$\Psi_{y>0}(y) = \begin{pmatrix} a \\ b \\ c \\ d \end{pmatrix} e^{-py}. \quad \text{(A21)}$$

A nontrivial solution of this type exists when p is a solution to the following characteristic equation:

$$\left[-C_2\left(p^2 - k_x^2\right) + C_1 k_z^2 + C_0 - E\right]^2 - \left[M_2\left(p^2 - k_x^2\right) + \gamma k_z^2 - \gamma m\right]^2 + v^2\left(p^2 - k_x^2\right) - \alpha^2 k_z^2\left(p^2 - k_x^2\right)^2 = 0. \quad \text{(A22)}$$

(Strictly speaking, the characteristic equation has the square on the left hand side, implying that the degeneracy of its solutions should be doubled.) This equation has *two* pairs of distinct solutions: $p = \pm p_1$ and $p = \pm p_2$, where

$$p_{1,2} = \sqrt{k_x^2 - \frac{X \pm \sqrt{X^2 + Y}}{2\left(M_2^2 - C_2^2 + \alpha^2 k_z^2\right)}}, \quad \text{(A23)}$$

cf. Eq. (A9). Here, the expression for X is the same as in the 2×2 model ($\alpha = 0$) in Eq. (A10), but the expression for Y is slightly different, i.e.,

$$Y \equiv 4\left(M_2^2 - C_2^2 + \alpha^2 k_z^2\right) \times\left[\left(C_1 k_z^2 + C_0 - E\right)^2 - \gamma^2\left(k_z^2 - m\right)^2\right]. \quad \text{(A24)}$$

Therefore, in the half-space occupied by the semimetal ($y > 0$), the wave function should have the following general

form:

$$\Psi_{y>0}(y) \simeq \begin{pmatrix} a_1 \\ Q_1^+ a_1 - T_1^+ c_1 \\ c_1 \\ -T_1^- a_1 + Q_1^- c_1 \end{pmatrix} e^{-p_1 y} + \begin{pmatrix} a_2 \\ Q_2^+ a_2 - T_2^+ c_2 \\ c_2 \\ -T_2^- a_2 + Q_2^- c_2 \end{pmatrix} e^{-p_2 y}, \tag{A25}$$

where we also introduced the shorthand notation: $Q_i^{\pm} \equiv Q(p_i, \pm k_x)$ and $T_i^{\pm} \equiv T(p_i, \pm k_x)$. Here the function $Q(p,k_x)$ is the same as in Eq. (A12) and

$$T(p,k_x) = \frac{\alpha k_z (p + k_x)^2}{-M_2\left(p^2 - k_x^2\right) - \gamma\left(k_z^2 - m\right) + vp}. \tag{A26}$$

In the vacuum solution ($y < 0$), we replace $m \to -\tilde{m}$ and take the limit $\tilde{m} \to \infty$. In this case, a simple analysis leads to the following solution:

$$\Psi_{y<0}(y) \simeq \frac{1}{\sqrt{\gamma\tilde{m}}} \begin{pmatrix} \tilde{a}_1 \\ \frac{\tilde{a}_1 C_2 + \alpha k_z \tilde{c}_1}{\sqrt{C_2^2 - \alpha^2 k_z^2}} \\ \tilde{c}_1 \\ \frac{\alpha k_z \tilde{a}_1 + C_2 \tilde{c}_1}{\sqrt{C_2^2 - \alpha^2 k_z^2}} \end{pmatrix} e^{\tilde{p}_1 y} + \frac{1}{\sqrt{\gamma\tilde{m}}} \begin{pmatrix} \tilde{a}_2 \\ -\frac{\tilde{a}_2 C_2 + \alpha k_z \tilde{c}_2}{\sqrt{C_2^2 - \alpha^2 k_z^2}} \\ \tilde{c}_2 \\ -\frac{\alpha k_z \tilde{a}_2 + C_2 \tilde{c}_2}{\sqrt{C_2^2 - \alpha^2 k_z^2}} \end{pmatrix} e^{\tilde{p}_2 y}, \tag{A27}$$

where, for convenience, we introduced an overall constant inversely proportional to $\sqrt{\gamma\tilde{m}}$. The explicit form of the exponents in this solution is determined by

$$\tilde{p}_1 \simeq \sqrt{\frac{\gamma\tilde{m}}{-M_2 + \sqrt{C_2^2 - \alpha^2 k_z^2}}}, \quad \tilde{p}_2 \simeq \sqrt{\frac{\gamma\tilde{m}}{-M_2 - \sqrt{C_2^2 - \alpha^2 k_z^2}}}. \tag{A28}$$

Note that the signs in the exponents of the vacuum solution (A27) are chosen so that the wave function vanishes at $y \to -\infty$.

The conditions of the continuity of the wave function in Eq. (A16) lead to the following constraints:

$$0 = Q_1^+ a_1 - T_1^+ c_1 + Q_2^+ a_2 - T_2^+ c_2, \tag{A29}$$

$$0 = T_1^- a_1 - Q_1^- c_1 + T_2^- a_2 - Q_2^- c_2, \tag{A30}$$

together with $a_2 = -a_1$ and $c_2 = -c_1$. Here, we took into account that the left hand side of Eq. (A16) vanishes in the limit $\tilde{m} \to \infty$.

As in the case of a two-component model, discussed in Appendix A 1, there is no need to satisfy the continuity conditions for the wave function derivatives, given by Eqs. (A17) through (A20). The reason is that these conditions add no additional constraints on the spinor solutions in the semimetal. They are needed only for determining the components of the vacuum solution at $y < 0$. Since the latter has no physical content in the limit $\tilde{m} \to \infty$, we can safely ignore the conditions in Eqs. (A17) through (A20). In order to have a nontrivial solution to Eqs. (A29) and (A30), the condition in Eq. (35) in the main text should be satisfied.

APPENDIX B: SYMMETRIES AND SURFACE FERMI ARCS BISPINORS

In this appendix, we discuss the properties of the Fermi arc surface states with respect to the discrete symmetries $U_\chi \equiv U\Pi_{k_z}$ and $\tilde{U}\Pi_{k_x}$, introduced in Sec. II B. To start with, let us note that the general Fermi arc spinor in Eq. (A25) contains all possible solutions. It is possible to classify these solutions with respect to the discrete symmetry U_χ by choosing them as eigenstates of the operator U_χ.

In order to construct the first group of solutions, we use the relations in Eqs. (A29) and (A30) and rewrite the Fermi arc spinor in Eq. (A25) in the following form:

$$\Psi_+ = a_1 \begin{pmatrix} 1 \\ Q_1^+ - T_1^+ \frac{T_1^- - T_2^-}{Q_1^- - Q_2^-} \\ \frac{T_1^- - T_2^-}{Q_1^- - Q_2^-} \\ -T_1^- + Q_1^- \frac{T_1^- - T_2^-}{Q_1^- - Q_2^-} \end{pmatrix} e^{-p_1 y} - a_1 \begin{pmatrix} 1 \\ Q_2^+ - T_2^+ \frac{T_1^- - T_2^-}{Q_1^- - Q_2^-} \\ \frac{T_1^- - T_2^-}{Q_1^- - Q_2^-} \\ -T_2^- + Q_2^- \frac{T_1^- - T_2^-}{Q_1^- - Q_2^-} \end{pmatrix} e^{-p_2 y}. \tag{B1}$$

By noting that p_i's (with $i = 1,2$), defined in Eq. (A23), contain only quadratic terms in momenta k_x and k_z, we conclude that both of them are invariant under the Π_{k_z} and Π_{k_x} transformations. The other quantities, used in Eq. (B1), transform as follows:

$$\Pi_{k_z} Q_i^{\pm} = Q_i^{\pm}, \quad \Pi_{k_z} T_i^{\pm} = -T_i^{\pm}, \tag{B2}$$

$$\Pi_{k_x} Q_i^{\pm} = Q_i^{\mp}, \quad \Pi_{k_x} T_i^{\pm} = T_i^{\mp}. \tag{B3}$$

It is straightforward to check that the spinor in Eq. (B1) is an eigenstate of the operator U_χ with the eigenvalue $\chi = +1$. Indeed, by making use of the definition of the matrix U, we find that

$$U\Psi_+ = a_1 \begin{pmatrix} 1 \\ Q_1^+ - T_1^+ \frac{T_1^- - T_2^-}{Q_1^- - Q_2^-} \\ -\left[\frac{T_1^- - T_2^-}{Q_1^- - Q_2^-}\right] \\ -\left[-T_1^- + Q_1^- \frac{T_1^- - T_2^-}{Q_1^- - Q_2^-}\right] \end{pmatrix} e^{-p_1 y} - a_1 \begin{pmatrix} 1 \\ Q_2^+ - T_2^+ \frac{T_1^- - T_2^-}{Q_1^- - Q_2^-} \\ -\left[\frac{T_1^- - T_2^-}{Q_1^- - Q_2^-}\right] \\ -\left[-T_2^- + Q_2^- \frac{T_1^- - T_2^-}{Q_1^- - Q_2^-}\right] \end{pmatrix} e^{-p_2 y}. \tag{B4}$$

Then, by taking into account that $U_\chi \equiv U\Pi_{k_z}$, we see that $U_\chi \Psi_+ = \Psi_+$, as claimed.

By using the relations in Eqs. (A29) and (A30), the Fermi arc spinor in Eq. (A25) can be also rewritten in the following alternative form:

$$\Psi_- = c_1 \begin{pmatrix} \frac{T_1^+ - T_2^+}{Q_1^+ - Q_2^+} \\ Q_1^+ \frac{T_1^+ - T_2^+}{Q_1^+ - Q_2^+} - T_1^+ \\ 1 \\ -T_1^- \frac{T_1^+ - T_2^+}{Q_1^+ - Q_2^+} + Q_1^- \end{pmatrix} e^{-p_1 y} - c_1 \begin{pmatrix} \frac{T_1^+ - T_2^+}{Q_1^+ - Q_2^+} \\ Q_2^+ \frac{T_1^+ - T_2^+}{Q_1^+ - Q_2^+} - T_2^+ \\ 1 \\ -T_2^- \frac{T_1^+ - T_2^+}{Q_1^+ - Q_2^+} + Q_2^- \end{pmatrix} e^{-p_2 y}. \tag{B5}$$

In this case, as is easy to check, the spinor is an eigenstate of the operator U_χ with eigenvalue $\chi = -1$. Indeed, by making use of the definition of the matrix U, we find that

$$U\Psi_- = c_1 \begin{pmatrix} \frac{T_1^+ - T_2^+}{Q_1^+ - Q_2^+} \\ Q_1^+ \frac{T_1^+ - T_2^+}{Q_1^+ - Q_2^+} - T_1^+ \\ -1 \\ -\left[-T_1^- \frac{T_1^+ - T_2^+}{Q_1^+ - Q_2^+} + Q_1^-\right] \end{pmatrix} e^{-p_1 y} - c_1 \begin{pmatrix} \frac{T_1^+ - T_2^+}{Q_1^+ - Q_2^+} \\ Q_2^+ \frac{T_1^+ - T_2^+}{Q_1^+ - Q_2^+} - T_2^+ \\ -1 \\ -\left[-T_2^- \frac{T_1^+ - T_2^+}{Q_1^+ - Q_2^+} + Q_2^-\right] \end{pmatrix} e^{-p_2 y}, \tag{B6}$$

which implies that $U_\chi \Psi_- = -\Psi_-$. In other words, the eigenstate Ψ_- corresponds to $\chi = -1$, as claimed.

Now, let us explore the implications of the $\tilde{U}\Pi_{k_x}$ symmetry in the model at hand. By applying the corresponding operator to the eigenstates $\Psi_\pm$, we arrive at the following results:

$$\tilde{U}\Pi_{k_x}\Psi_+ = a_1 \begin{pmatrix} \frac{Q_1^- - Q_2^-}{T_1^- - T_2^-} \\ -T_1^+ + Q_1^+ \frac{Q_1^- - Q_2^-}{T_1^- - T_2^-} \\ 1 \\ Q_1^- - T_1^- \frac{Q_1^- - Q_2^-}{T_1^- - T_2^-} \end{pmatrix} e^{-p_1 y} - a_1 \begin{pmatrix} \frac{Q_1^- - Q_2^-}{T_1^- - T_2^-} \\ -T_2^+ + Q_2^+ \frac{Q_1^- - Q_2^-}{T_1^- - T_2^-} \\ 1 \\ Q_2^- - T_2^- \frac{Q_1^- - Q_2^-}{T_1^- - T_2^-} \end{pmatrix} e^{-p_2 y}, \tag{B7}$$

$$\tilde{U}\Pi_{k_x}\Psi_- = c_1 \begin{pmatrix} 1 \\ -T_1^+ \frac{T_1^- - T_2^-}{Q_1^- - Q_2^-} + Q_1^+ \\ \frac{T_1^- - T_2^-}{Q_1^- - Q_2^-} \\ Q_1^- \frac{T_1^- - T_2^-}{Q_1^- - Q_2^-} - T_1^- \end{pmatrix} e^{-p_1 y} - c_1 \begin{pmatrix} 1 \\ -T_2^+ \frac{T_1^- - T_2^-}{Q_1^- - Q_2^-} + Q_2^+ \\ \frac{T_1^- - T_2^-}{Q_1^- - Q_2^-} \\ Q_2^- \frac{T_1^- - T_2^-}{Q_1^- - Q_2^-} - T_2^- \end{pmatrix} e^{-p_2 y}. \tag{B8}$$

These results show that $\Psi_\pm$ are not eigenstates of the operator $\tilde{U}\Pi_{k_x}$. However, by taking into account the constraint in Eq. (35), one can check that the operator $\tilde{U}\Pi_{k_x}$ interchanges the two types of the states, i.e., $\Psi_+ \leftrightarrow \Psi_-$.

In conclusion, the results of this Appendix confirm the claim in the main text of the paper concerning the symmetry properties of the low-energy theory for A_3Bi (A = Na, K, Rb) semimetals, as well as the classification of their Fermi arc states. These are in complete agreement with the claim that the corresponding compounds are $\mathbb{Z}_2$ Weyl semimetals.

[1] K. S. Novoselov, A. K. Geim, S. V. Morozov, D. Jiang, Y. Zhang, S. V. Dubonos, I. V. Grigorieva, and A. A. Firsov, Science **306**, 666 (2004).

[2] S. M. Young, S. Zaheer, J. C. Y. Teo, C. L. Kane, E. J. Mele, and A. M. Rappe, Phys. Rev. Lett. **108**, 140405 (2012).

[3] J. L. Manes, Phys. Rev. B **85**, 155118 (2012).

[4] Z. Wang, Y. Sun, X. Q. Chen, C. Franchini, G. Xu, H. Weng, X. Dai, and Z. Fang, Phys. Rev. B **85**, 195320 (2012).

[5] Z. Wang, H. Weng, Q. Wu, X. Dai, and Z. Fang, Phys. Rev. B **88**, 125427 (2013).

[6] S. Borisenko, Q. Gibson, D. Evtushinsky, V. Zabolotnyy, B. Buchner, and R. J. Cava, Phys. Rev. Lett. **113**, 027603 (2014).

[7] M. Neupane, S.-Y. Xu, R. Sankar, N. Alidoust, G. Bian, C. Liu, I. Belopolski, T.-R. Chang, H.-T. Jeng, H. Lin, A. Bansil, F. Chou, and M. Z. Hasan, Nat. Commun. **5**, 3786 (2014).

[8] Z. K. Liu, B. Zhou, Y. Zhang, Z. J. Wang, H. M. Weng, D. Prabhakaran, S.-K. Mo, Z. X. Shen, Z. Fang, X. Dai, Z. Hussain, and Y. L. Chen, Science **343**, 864 (2014).

[9] A. A. Burkov, M. D. Hook, and L. Balents, Phys. Rev. B **84**, 235126 (2011).

[10] A. M. Turner and A. Vishwanath, arXiv:1301.0330 [cond-mat.str-el].

[11] O. Vafek and A. Vishwanath, Ann. Rev. Condens. Mattter Phys. **5**, 83 (2014).

[12] X. Wan, A. M. Turner, A. Vishwanath, and S. Y. Savrasov, Phys. Rev. B **83**, 205101 (2011).

[13] A. A. Burkov and L. Balents, Phys. Rev. Lett. **107**, 127205 (2011).

[14] G. Y. Cho, arXiv:1110.1939 [cond-mat.str-el].

[15] H. Weng, C. Fang, Z. Fang, B. A. Bernevig, and X. Dai, Phys. Rev. X **5**, 011029 (2015).

[16] S.-M. Huang, Su-Y. Xu, I. Belopolski, C.-C. Lee, G. Chang, B. Wang, N. Alidoust, G. Bian, M. Neupane, A. Bansil, H. Lin, and M. Z. Hasan, arXiv:1501.00755 [cond-mat.mtrl-sci].

[17] C. Zhang, Z. Yuan, S. Xu, Z. Lin, B. Tong, M. Z. Hasan, J. Wang, C. Zhang, and S. Jia, arXiv:1502.00251 [cond-mat.mtrl-sci]

[18] S.-Y. Xu, I. Belopolski, N. Alidoust, M. Neupane, C. Zhang, R. Sankar, S.-M. Huang, C.-C. Lee, G. Chang, B. Wang, G. Bian, H. Zheng, D. S. Sanchez, F. Chou, H. Lin, S. Jia, and M. Z. Hasan, arXiv:1502.03807 [cond-mat.mtrl-sci].

[19] B. Q. Lv, H. M. Weng, B. B. Fu, X. P. Wang, H. Miao, J. Ma, P. Richard, X. C. Huang, L. X. Zhao, G. F. Chen, Z. Fang, X. Dai, T. Qian, and H. Ding, arXiv:1502.04684 [cond-mat.mtrl-sci].

[20] X. Huang, L. Zhao, Y. Long, P. Wang, D. Chen, Z. Yang, H. Liang, M. Xue, H. Weng, Z. Fang, X. Dai, and G. Chen, arXiv:1503.01304 [cond-mat.mtrl-sci].

[21] L. Lu, Z. Wang, D. Ye, L. Ran, L. Fu, J. D. Joannopoulos, and M. Soljačić, arXiv:1502.03438 [cond-mat.mtrl-sci].

[22] E. V. Gorbar, V. A. Miransky, and I. A. Shovkovy, Phys. Rev. B **88**, 165105 (2013).

[23] H.-J. Kim, K.-S. Kim, J. F. Wang, M. Sasaki, N. Satoh, A. Ohnishi, M. Kitaura, M. Yang, and L. Li, Phys. Rev. Lett. **111**, 246603 (2013).

[24] E. V. Gorbar, V. A. Miransky, and I. A. Shovkovy, Phys. Rev. B **89**, 085126 (2014).

[25] D. T. Son and B. Z. Spivak, Phys. Rev. B **88**, 104412 (2013).

[26] H. B. Nielsen and M. Ninomiya, Phys. Lett. B **130**, 389 (1983).

[27] F. D. M. Haldane, arXiv:1401.0529 [cond-mat.str-el].

[28] V. Aji, Phys. Rev. B **85**, 241101 (2012).

[29] R. Okugawa and S. Murakami, Phys. Rev. B **89**, 235315 (2014).

[30] P. Hosur, Phys. Rev. B **86**, 195102 (2012).

[31] A. C. Potter, I. Kimchi, and A. Vishwanath, Nat. Commun. **5**, 5161 (2014).

[32] E. V. Gorbar, V. A. Miransky, I. A. Shovkovy, and P. O. Sukhachov, Phys. Rev. B **90**, 115131 (2014).

[33] E. V. Gorbar, V. A. Miransky, I. A. Shovkovy, and P. O. Sukhachov, Phys. Rev. B **91**, 121101 (2015).

[34] W. Zhang, R. Yu, H. J. Zhang, X. Dai, and Z. Fang, New J. Phys. **12**, 065013 (2010).

[35] S. Q. Shen, *Topological Insulators* (Springer, Heidelberg, 2012).

[36] S.-Y. Xu, C. Liu, S. K. Kushwaha, R. Sankar, J. W. Krizan, I. Belopolski, M. Neupane, G. Bian, N. Alidoust, T.-R. Chang, H.-T. Jeng, C.-Y. Huang, W.-F. Tsai, H. Lin, P. P. Shibayev, F.-C. Chou, R. J. Cava, and M. Z. Hasan, Science **347**, 294 (2015).